Investigation of Low-Voltage Pulse Parameters on Electroporation and Electrical Lysis Using a Microfluidic Device With Interdigitated Electrodes

Bashir I. Morshed*, *Member, IEEE*, Maitham Shams, and Tofy Mussivand

***Abstract*—Electroporation (EP) of biological cells leads to the exchange of materials through the permeabilized cell membrane, while electrical lysis (EL) irreversibly disrupts the cell membrane. We report a microfluidic device to study these two phenomena with low-voltage excitation for lab-on-a-chip (LOC) applications. For systematic study of EP, we have employed a quantification metric: flow Index (FI) of EP. Simulation and experimental results with the microfluidic device containing interdigitated, coplanar, integrated electrodes to electroporate, and rapidly lyse biological cells are presented. H&E stained human buccal cells were subjected to various pulse magnitudes, pulsewidths, and number of pulses. Simulations show that an electric field of 25 kV/cm with a 20 V applied potential produced 1.3 °C temperature rise for a 5 s of excitation. For a 20 V pulse-excitation with pulse-widths between 0.5 to 5 s, EL was observed, whereas for lower excitations, only EP was observed. FI of EP is found to be a direct function of pulse magnitudes, pulsewidths, and numbers of pulses. To release DNA from nucleus, excitation-pulses of 5 s were required. Quantification of EP would be useful for systematic study of EP toward optimization with various excitation pulses, while low-voltage requirement and high yield of EP and EL are critical to develop LOC for drug delivery and cell-sample preparation, respectively.**

***Index Terms*—Electric field, electrical lysis (EL), electroporation (EP), flow index of electroporation, microfluidic device.**

I. Introduction

PLASMA membrane of a cell is a 5 to 8 nm thick protein-lipid bilayer, and forms a physical barrier separating cell contents from the extracellular environment [1]. Permeabilization or breaking down of the plasma membrane is necessary for many applications based on lab-on-a-chip (LOC) technology. When a cell is placed inside an electric field, charges accumulate along the plasma membrane, inducing a potential across the membrane [2]. The induced membrane potential causes an electrical force on bilayer phospholipids (e.g., 1,2-dimyristoyl-sn-Glycero-3-phosphorylcholine, DMPC), and exerts a stress for reorientation due to electric dipole properties [3]. If the applied electric field is increased such that the induced membrane potential reaches a critical value of 1 V, these dipoles undergo conformal changes in membrane structure causing formation of a large number of hydrophilic pores or channels through the plasma membrane [4]–[6]. This phenomenon of numerous reversible pore formation in the plasma membrane, due to a high electric field of intensity in several kV/cm and duration of μs-to-ms, is known as electroporation (EP) [7], [8]. This induces a temporary loss of semipermeability of plasma membrane, and can cause in ion leakage, escape of metabolites, selective release of intracellular molecules, and increased uptake of drugs, molecular probes, and genetic materials [8]–[15]. Medical applications include controlled drug delivery, gene transfection, and vascular therapy [16].

If the electric field is sustained for a critical duration, cell membrane completely disintegrates, causing cell lysis [17]–[28], a process of breaking a open cell through rupturing this cellular plasma membrane by external physical or chemical stimulus, releasing the contents of the cell including deoxyribonucleic acid (DNA) [29], [30]. Other methods for lysis include mechanical shear [31], liquid shear [32], gaseous shear [33], osmotic pressure [34], electroosmotic [35], sonication [36], chemical stimulus [37] using nonionic detergents and lysis agents, e.g., Chelex, QIAamp [1], [37]–[39], laser [40], [41], and thermal [42], [43] stimulations. Electrical lysis (EL), a rapid mechanism, on a microfluidic platform can be used for biodefense and diagnostic systems [44]. EP and EL of biological cells on microfluidic chips are of recent interest due to simple, low-cost device, and fast operation [8], [17].

A major challenge of studying EP and EL is the lack of any systematic quantitative metric that will allow comparative study of experiments and improve classification in describing the severity. EP and EL are known to be dependent on various parameters including the electrical excitation durations, electric field magnitudes, number of excitation pulses, frequency, orientations of the electric field, cell size and shape, as well as buffer osmolarity and conductivity [45]–[49]. The majority of studies have quantified EP through the percentage of cells undergoing EP detected by stain uptake [50], and percentage of fluorescent cells [51], [52]. An indirect approach to quantify severity of EP is detection of increase in transmembrane conductance that increases conductance with higher electric field or increasing number of pulses [46]. Some approaches are critically cell-size

Manuscript received July 9, 2013; revised September 15, 2013; accepted October 28, 2013. Date of publication November 20, 2013; date of current version February 14, 2014. This work was supported by the Canadian Microelectronics Corporation. *Asterisk indicates corresponding author.*

*B. I. Morshed is with the Department of Electrical and Computer Engineering, University of Memphis, Memphis, TN 38152 USA (e-mail: bmorshed@memphis.edu).

M. Shams is with the Electronics Department, Carleton University, ON K1S 5B6, Canada (e-mail: shams@doe.carleton.ca).

T. Mussivand is with the Medical Devices Innovation Institute, University of Ottawa, Ottawa, ON K1N 6N5, Canada (e-mail: tmussivand@ottawaheart.ca).

Color versions of one or more of the figures in this paper are available online at http://ieeexplore.ieee.org.

Digital Object Identifier 10.1109/TBME.2013.2291794

dependent such as determining the amounts of stains uptake per cell after a certain number of cell lysis and measurement of stains with a calibrated microscope [53], and the percentage of area coverage by stained cells after EP [54]. Other quantification approaches are critically time dependent such as determining the delivery rate [55] and transfection rate [56].

The applied potential required for EL of protoplast cells and other plant cells were demonstrated to be as low as 10 to 30 V that generated electric field between 1 to 10 kV/cm [19], [57]. Human cells, such as breast cancer cells, require higher potential and electric field; such as 40 V to generate around 20 kV/cm as reported by Nashimoto [58]. Release of intracellular molecules through EL has been reported such as genetic materials and ribonucleic acid (RNA) [58]. Lu *et al.* showed human colon carcinoma can be lysed inside microchannels that released nucleus [22]. Munce *et al.* demonstrated that EL can extract cell contents within cytoplasm [59]. Marc *et al.* demonstrated EL releases oregon green and fluorescein dye from cells [60]. Rosa *et al.* and Park *et al.* reported release of DNA from bordetella pertussis and vaccinia virus, respectively; none of those has nucleus [61], [62]. Nanosecond pulses have been shown to affect only intracellular membranes without rupturing cell membranes [63].

For low-voltage EP and EL, we report a novel microfluidic device with integrated coplanar interdigitated electrodes, along with top cell-loading ports that increases throughput and reusability. Furthermore, to quantify the severity of EP, we apply a quantitative image analysis approach along with a quantification metric: flow index (FI) of EP [64]. This enables us to perform quantitative comparison for systematic analysis. We hypothesize that disintegration of nuclear membrane will require application of pulses with higher energy. We experimentally show that EL of human cell can be performed with low voltage excitation and longer pulse duration. DNA release by rupturing the nuclear membrane requires pulses with even longer durations containing higher energy.

II. Materials and Methods

A. Microfluidic Device Design, Fabrication, and Postprocessing

The microfluidic device was designed using MEMSPro version 5.1 (SoftMEMS, CA, USA). The device housed a microfluidic chamber for EP and EL composed of five parallel microchannels. Each microchannel was 12 mm long, 400 μm wide, and 40 μm deep. These microchannels merged at both ends and terminated at two fluidic ports. The device also contained an integrated electrode layer. To generate an electric field inside the microchannel, this layer was utilized to design interdigitated fingers of 420 μm length and 10 μm width at the bottom of each microchannel placed perpendicular to the axis of the microchannel (see Fig. 1). The gaps between fingers were 10 μm. The fingers were alternatively connected to two thick electrodes of 0.5 mm width on both sides of the microchannel, thus forming an interdigitated configuration. The thick electrodes connected the fingers with two electrode ports. There were 31 cell loading ports directly above the microchannels to

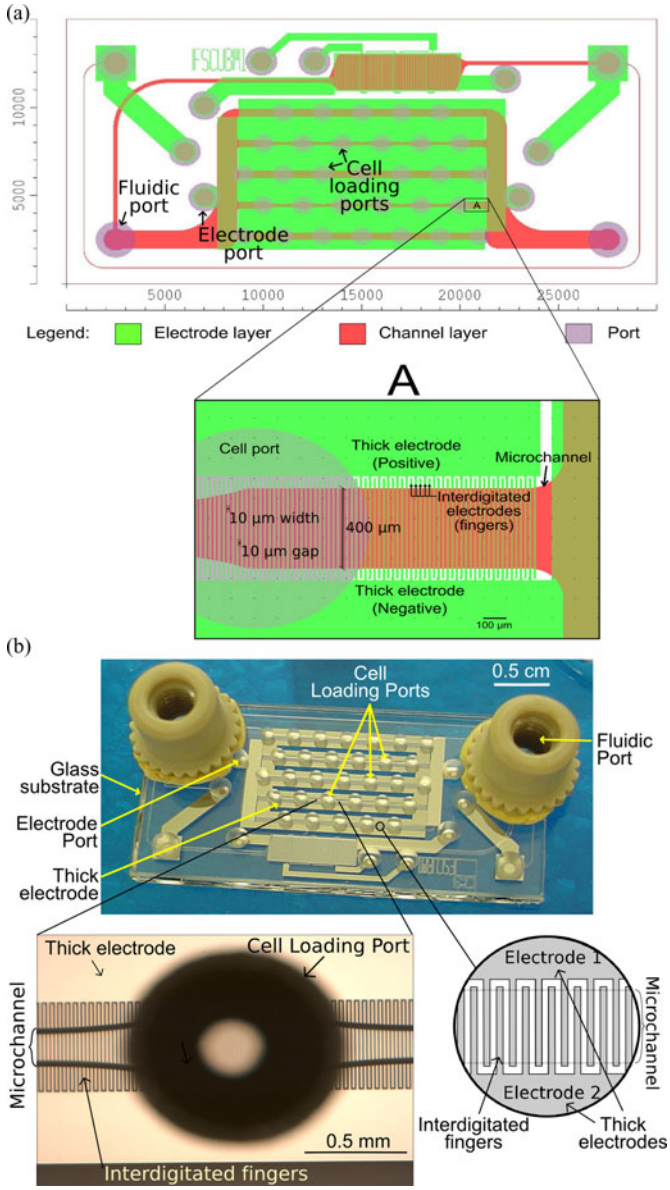

Fig. 1. (a) Layout of the microfluidic device with enlargement of a section (A) of the microfluidic chamber. (b) Photograph of the prototyped device after postprocessing, with an inset depicting an optical microscope image of a cell loading port, a portion of a microfluidic channel and interdigitated electrodes, while another inset showing the interdigitated electrode design.

quickly load samples. The chip layout contains three mask layers: electrode mask (labeled green), microchannel mask (labeled red), and port mask (labeled green) as shown in Fig. 1(a). Note that the overlap of two different layers depicts as a yellowish color. The chip boundary is shown with the brown rectangle, and the adjacent scale is in micron. Three types of ports were designed for fluidic access (fluidic port, $\phi = 1.5$ mm), electrical access (electrode port, $\phi = 1.2$ mm), and sample cell access (cell loading port, $\phi = 1$ mm). The cell loading ports were directly above the five parallel microchannels of the chamber, and were laterally spaced by 2 mm.

The microfluidic device was fabricated through SensoNit Fabrication Process (Micronit, Inc., The Netherlands). The chip

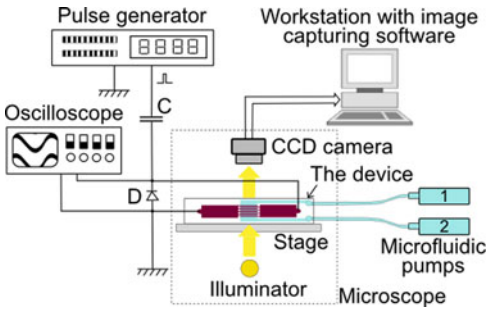

Fig. 2. Schematic diagram of the experimental setup of the microfluidic device connected to a pulse generator and an oscilloscope through a capacitor (C) and a diode (D). The fluidic path is indicated in blue, while the optical path is indicated in yellow.

comprised of two glass slides of 1.1 and 0.7 mm thickness as substrates. The top slide contained the ports and the bottom slide contained the microchannel and the integrated electrodes. The fabrication process involved creation of trenches through wet chemical etching for microchannels using channel mask, then the deposition of electrode materials using sputter coating technique inside 200 nm deep cavities etched at the bottom of the trenches using electrode mask. The electrodes composed of 180 nm thick platinum (Pt) layer on top of 20 nm thick tantalum (Ta), which serves as the adhesion layer between the Pt and the etched glass surface. Ports were created on the top slide with powder blasting technique using port mask. The two glass slides were aligned and thermally fused. The fabricated device was 3 cm long, 1.5 cm wide, and 1.8 mm thick. A microscopic image of a microchannel, a cell loading port, and the interdigitated integrated electrodes within the microfluidic chamber of the fabricated device is shown in Fig. 1(b).

Postprocessing involved fixation of fluidic and electrical connectivities. Nanoport assemblies (Upchurch Scientific, WA, USA) were affixed on top of the fluidic ports for fluidic access through capillary tubing connections. External electrodes were connected to the integrated electrodes through the electrode ports using silver conductive epoxy (Cat. 8331-14G, MG Chemicals, ON, Canada). A photograph of the postprocessed device is shown in Fig. 1(b). For initial wetting of the microchannel surfaces, a 10% detergent solution (Triton X-100, Thermo Fisher Scientific, MA, USA) was introduced inside the microchannels and washed thoroughly with ddH_2O.

B. Experimental Setup

The schematic diagram of the experimental setup is shown in Fig. 2. As the source of electrical excitation, a pulse generator (HP33120A, Hewlett-Packard Company, CA, USA) was used. An oscilloscope (TDS-3012, Tektronix, Inc., OR, USA) was used to monitor and record the pulse waveform. A capacitor, C, of 1 μF (SN010M050ST, Cornell Dubilier, SC, USA) was included in series of the pulse generator to block any dc offset voltage while passing the pulse excitation; hence reducing power loss, electrode degradation, and increasing fault tolerance of the experimental setup. A reverse-biased diode, D, (IN4007, Texas Instruments, TX, USA) was connected across the electrode ports to limit the residual voltage developed across the fingers inside the microchannels. Two syringe pumps (Cat. 780100C, Cole-Parmer, IL, USA) were used to introduce (or to remove) buffer fluids inside the microchannels through the fluidic ports. The test-fixture included a clean glass slide of dimension 75 mm $\times$ 25 mm (Cat. 12-550-15, Fisher Scientific, PA, USA) on which the fabricated and postprocessed device was secured using silicone to enable proper positioning on the microscope stage. As the fluidic ports provided open fluidic paths for buffer, fluid loading (and removal) was performed through both syringe pumps in the same operating mode (i.e., loading mode or removal mode). Experiments were performed on the stage of an optical microscope (CKX41, Olympus Corp., IL, USA) with an integrated charge-coupled device (CCD) camera to capture the sequence of images at every 0.5 s interval starting from the pulse excitation. The CCD camera was connected to a workstation with ImagePro Express software (Media Cybernetics, Inc., MD, USA) that acquired and saved the image sequences.

C. Cell Sample Preparation

Sample cells were collected noninvasively using buccal swabs from volunteers and stained using both Haematoxylin (Cat. 3530-16, Ricca Chemical, TX, USA) and Eosin Y (Cat. SE22-500D, Fisher Chemical, PA, USA) stains (known as H&E staining). The average diameter of the sample cells were 40 μm and approximate concentration of a thousand cell/mL. Haematoxylin stain colors basophilic structures (such as chromosomes) with blue-purple hue. Eosin Y stain colors eosinophilic structures (like cytoplasm) in bright pink or magenta. A centrifuge-based method for freely flowing cell staining was developed, where the protocol replaces the conventional washing step with several "centrifuge-and-discard supernatant" steps. Briefly, the procedure involved washing sample cells to centrifuge tubes with 2 mL of deionized H_2O. Then, 10 μL of Haematoxylin and 20 μL of Eosin Y stain were added successively after centrifugation at 2000 r/min for 5 min then discarding the supernatant for three times. Stained sample cells were stored in a dark shelf and used within several days. The concentrations of the cells in samples were very low ($\sim$100 cells per mL). After staining process, there was no noticeable degradation of stains even after 1 week [64].

D. Experimentation Procedure

Prior to an experiment, the device was washed thoroughly with flowing ddH_2O and then dried with blowing hot air. The device was then secured on the stage of a microscope. Fluidic ports were connected to the syringe pumps through the capillary tubes and the external electrodes were connected to the pulse generator as shown in Fig. 2. The pumps were engaged to inject 10 μL of buffer fluids inside the microchannels at the rate of 50 μL/min. When the microfluidic chamber was filled with the introduced buffer fluid, the pumps were disengaged. After the buffer fluid flow was stopped, a 5 μL of the stained cell-sample solution was introduced in the microfluidic chamber through the cell loading ports by using a micropipette. Then, the cells

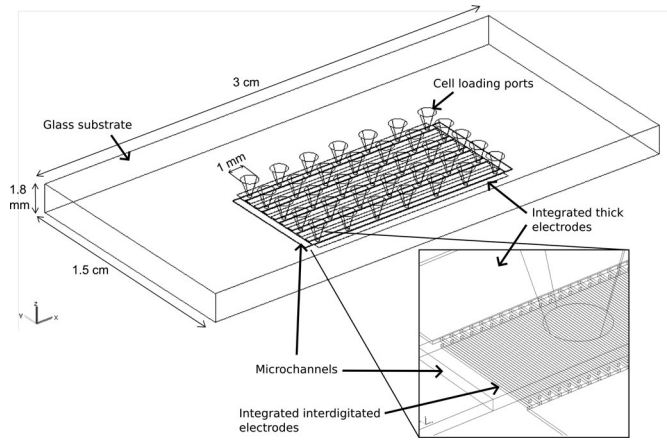

Fig. 3. 3-D model of the microfluidic device containing microchannel of the microfluidic chamber, integrated electrodes, and loading ports used for electric field and thermal simulations. The inset shows the interdigitated fingers at the bottom of a microchannel.

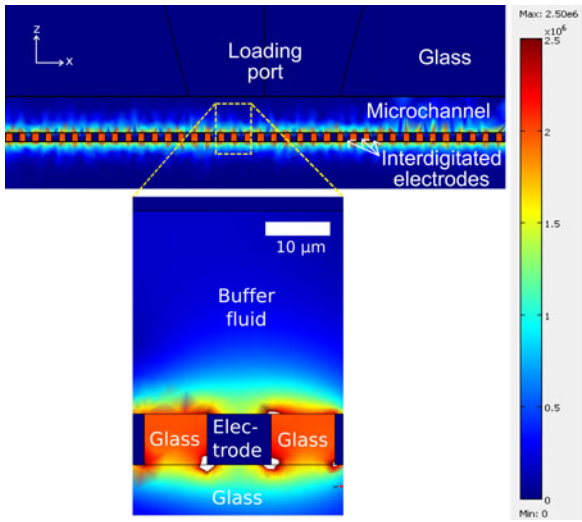

Fig. 4. FEM simulation of electric field of the model along xz-plane with a section enlarged to show distribution of electric fields.

were allowed 30 s to settle at the bottom of the microchannel. The focal plane of the microscope was fine-tuned such that some of the stained cells inside the chamber can be clearly observed through the CCD camera. The pulse excitation and the image capture sequence were initiated at the same instance. For EP experiments, excitation pulse magnitudes ranged from 2.5 to 20 V, resulting in estimated electric fields between 2.5 to 20 kV/cm. The pulse-width range was between 1 μs to 5 s, and the number of pulses was between 1 to 100. The rising edge of the initial pulse triggered the oscilloscope to capture the pulse waveform. The image capturing system saved the sequence of images in the hard disk of the workstation. For EL experiments, single pulses of long durations were investigated. The fluid after the pulse treatment was collected using a micropipette through the cell loading ports and observed under a 100$\times$ magnification oil-immersion optical microscope.

III. Results: Simulation

A. Model of the Microfluidic Device

Analysis of the developed electric fields and temperature rise inside the microchannels within the microfluidic chamber of the device was performed with finite element method (FEM) using Comsol Multiphysics software (Comsol, Inc., Burlington, MA, USA). The model of the essential components of the microdevice was generated using the 3-D Modeler (see Fig. 3). The material parameters were from Comsol Multiphysics Material Database available with the software. The model was meshed with a maximum growth rate of 1.3 resulting in 2258 159 tetrahedron elements with 385 863 mesh points and 3045 076 degrees of freedom.

B. Electric Field Simulations

Electric field simulations were performed using conductive dc media physics. The positive and negative electrodes were excited by applying potentials of 20 and 0 V, respectively. The boundary conditions for all external surfaces were set to electrical insulation, and all internal boundaries were electrical continuity. Isotropic conductivity was selected for all materials. Simulations were performed iteratively until the relative error converged below 0.1, while the absolute error tolerance was 0.01. A representative result is shown in Fig. 4 depicting the distribution of electric fields for excitation potential of 20 V. The peak electric fields inside the microfluidic chamber reached up to 25 kV/cm. The electric field near the electrodes at the bottom of the microchannel were higher. This is advantageous as cell samples were allowed to settle near the bottom of the microchannel after loading inside of the microfluidic chamber, due to the average density of cell ($\sim$1.5 gm/cm^3) to be higher then the density of the medium ($\sim$1 gm/cm^3). Portions of the cells away from the electrodes by 10 μm or more along z-axis might not experience the critical electric field for poration.

C. Thermal Simulations

Application of electrical current through the buffer fluid causes generation of heat (primarily Joule heating). The upper bound of such heat can be obtained by assuming that all power consumed in the microfluidic device has been dissipated as heat resulting in a heat generation ($Q = V \times I$), where V is the applied potential and I is the current flow. The general heat transfer physics was applied to simulate conductive and convective heat transfer of the materials, and heat radiation is ignored for a conservative estimate.

The device delivering 20 V resulted 1 V drop across a 50 Ω internal resistance of the power supply (based on empirical data). The calculated internal resistance of the buffer fluid is 1 kΩ, the average current flow is 20 mA, and power dissipation is 0.4 W inside the five microchannel paths. Hence, the average power dissipation in each microchannel is 0.08 W. With a 25% upper bound tolerance, a power dissipation of 0.1 W for each microchannel path was simulated. The heat generation per unit volume was calculated by dividing the power dissipation in the volume of that microchannel, and used as the volumetric

heat source. Transient analysis was performed using generalized minimal residual solver. The relative error tolerance for convergence was 0.01, while the absolute tolerance was 0.001. With these criteria, the obtained simulation results served as a conservative estimate of the temperature rise for electric current. The initial temperatures of all subdomains were set to 300°K (for room temperature of 26.8 °C). The temperature at infinite was set to 298°K. All internal boundaries were set to thermal conductivity while all external boundaries were set to convective heat flux dissipation with the heat transfer coefficient h of 5, 10, and 20 W/m^{2}K, as the range of h is typically between 4.4 to 32.2 W/m^{2}K corresponding to stationary air to forced air cooling, respectively. Theoretical calculation with an airflow rate of 1 m/s provides a heat transfer coefficient of 22.4 W/m^{2}K. The approach provides an estimate with reduced computational complexity [22], [65]–[67].

The transient thermal simulation for 5 s pulsewidth resulted a maximum temperature rise of 1.3°K of the fluid inside the microchannels of the chamber and the temperature increased to 2.2°K after 10 s of continuous excitation as shown in Fig. 5(a). The maximum temperate was observed at the middle of the microchannel under the loading ports, resulting from convection flow of water with higher temperature toward the opening of the loading port. Transient simulations over 10 s period for h values of 5, 10, and 20 W/m^{2}K are plotted in Fig. 5(b). The temperature rises were below 2.9°K for all cases for up to 10 s of excitation. For instance, with an excitation of 5 s duration, the rises of temperature were 1.7, 1.45, and 1.3 °C for h of 5, 10, and 20 W/m^{2}K, respectively. These thermal simulations indicate that the upper bound of temperature rise due to the electrical excitation was insignificant to cause damage of cells. These results are also in agreement with literatures that indicate a typical temperature rise due to Joule heating in buffer fluids are within several degrees [15], [22]. As biological cells can sustain a larger range of temperature variation in nature (typically up to 10 °C), this temperature rise due to the excitation is not expected to cause any significant change of cells. For thermal lysis, the required temperature is 70 to 80 °C [42], well beyond the temperature rise from these electric pulse stimulations.

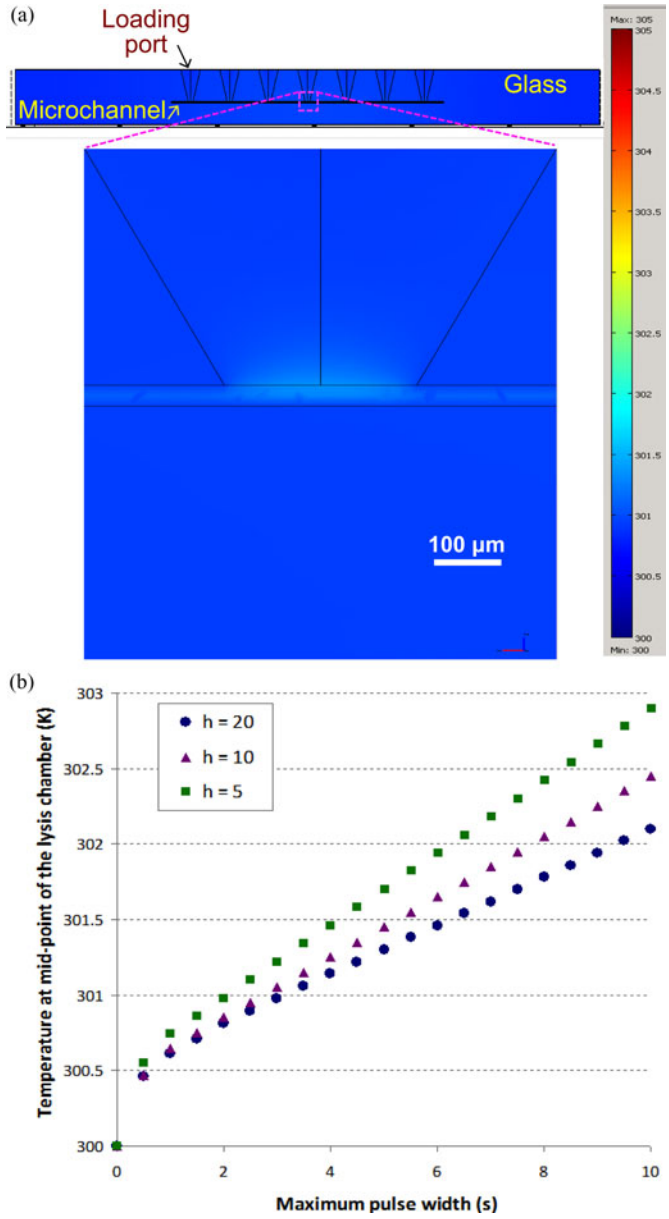

Fig. 5. (a) Temperature inside the microchannel visualized along xz-plane after electrical excitation of 20 V for 10 s. A section of the channel is enlarged to depict the corresponding temperature distribution. (b) Plot of transient increase of temperature for the heat transfer coefficient (h) of 5, 10, and 20 W/m^2 K, for an electric excitation of 20 V for 10 s. The initial temperature of all subdomains were at the room temperature of 300°K.

IV. Results: Experimental

A. Excitation Parameters

Experiments were conducted over a range of applied pulse parameters, such as magnitudes (from 2.5 to 20 V), pulsewidths (from 1 μs to 5 s), and numbers of pulses (from 1 to 100 pulse) to determine the effect of pulse parameters on EP and EL. Initial results have been reported elsewhere [64].

B. Image Processing for Quantification of EP

The image sequences captured from the experiments show stain reduction inside the sample cells after the application for various electrical excitations. The amounts of stain reduction were dependent on the applied pulse parameters. A representative example is shown in Fig. 6, where the set of images was captured at 0 and 145 s after a single pulse excitation of 1 ms duration and 5 V magnitude. The estimated maximum electric field was 5 kV/cm. The observation of reduction of Eosin Y stain suggests occurrence of EP, as stain of cytoplasm (Eosin Y) is diluted through the pores formed during EP (either by fluids exiting the cell and reducing stains within cells, or surrounding fluid entering the cell and reducing stain concentration in cells) [50], [53], [54]. Haematoxylin stain, on the other hand, has not reduced, suggesting that the chromosomes have not exited from the cell. It is evident that performing this type of qualitative analysis is challenging for comparison with other experimental cases. To allow quantitative analysis, the following approach was followed.

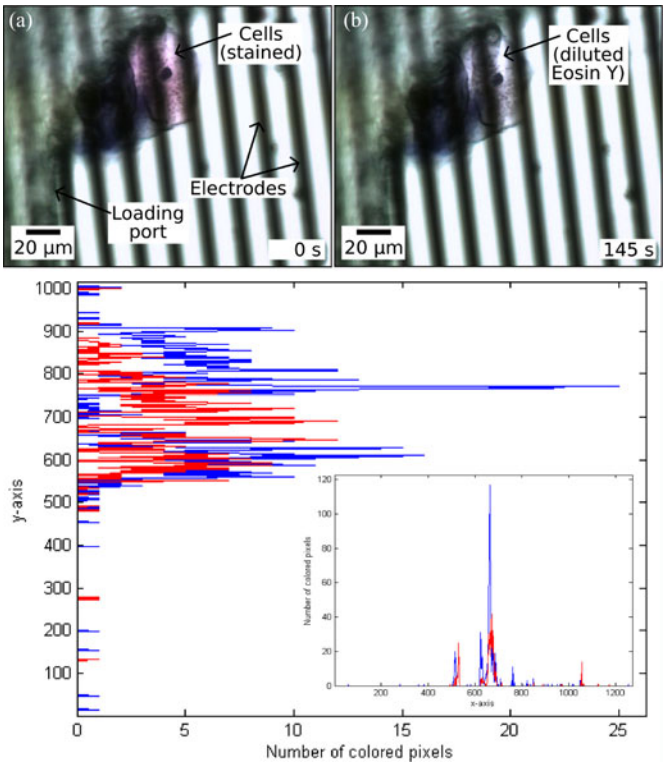

Fig. 6. (a-b) A set of images from EP experiments, followed by plots of extracted pixel data, for both the y-axis (plot below) and the x-axis (inset), from the pair of images captured at (a) 0 s, and (b) 145 s after the application of a 5 V, 1 ms pulse. Pixel data for Eosin Y from (a) are plotted with blue, while data from (b) are plotted with red. Decreased number of pixel data in red demonstrates a dilution of Eosin Y stained pixels due to EP. A temporal NSP plot would show a gradual decrease of NSP as provided in [64], [68].

The captured images were analyzed using software codes written in Visual Basic and MATLAB for quantitative analysis. The procedure is described elsewhere [68], and are mentioned briefly here. First, the frames were extracted in bitmap (BMP) format from the captured image sequence. Each pixel represented by a set of (R,G,B) values within a "color cube," where the stain color range of Eosin Y is approximated as the region of interest (ROI) [68]. The Visual Basic code determined the number of pixels within the ROI in each BMP file. The MATLAB script plotted these pixel data for each row or column in an image, or the total number of pixel data for a sequence of images against elapsed time. The images from a representative experiment are shown in Fig. 6 as an illustration.

The temporal plot of the total number of stained pixels provides quantitative measure of stain reduction due to EP. To be able to compare results from various experiments with different excitation parameters, all stained pixel data need to be normalized with respect to the number of stained pixels in the first image of the sequence. This will eliminate the bias on the initial state (e.g., number, size) of stained cells within the image sequence. The normalized value of the total stained pixels of each image is calculated by dividing the total number of stained pixels of an image by the total number of stained pixels of the first image of that sequence. This parameter is denoted by normalized stained pixel (NSP) [64]. Mathematically,

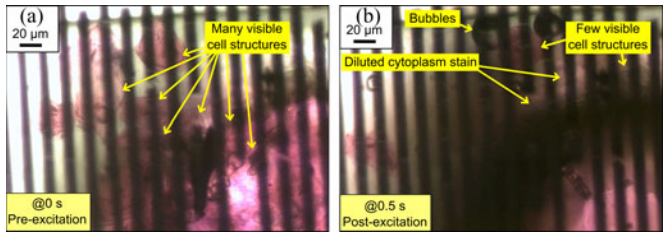

Fig. 7. Cell structures were broken and cytoplasm released to buffer medium as a pulse of 20 V magnitude and 500 ms duration was applied. The release of cytoplasm concluded from the diffused Eosin Y stains observed in (b).

$$\text{NSP} = \frac{\text{Number of stained pixels in an image of the sequence}}{\text{Number of stained pixels in the first image of the sequence}}. \quad (1)$$

For EP, the gradual decrease of NSP of exponential patterns was observed [64], [68].

C. Observations

If the change of NSP reduction at the end of observation (145 s) was less than 5%, then the excitation was considered to cause no effect. If the reduction of stain was higher, but cell membrane was not disintegrated (visually), then the excitation was considered to cause EP. Finally, if the cell membranes were broken or cell structures disintegrated, the excitation was considered to cause EL. A summary of all experimental observations is tabulated in Table I.

The experimental results demonstrated that a single pulse caused higher impact on the cell membrane compared to a pulse train delivering the same total amount of energy. Hence, for EL experiments, only single pulses were considered. As EL requires high energy pulses with the electric field above the critical level and pulsewidth larger than the critical time duration, all EL events were observed on the upper right hand corner of the energy-space plot (discussed later in Section V). Such pulses cause substantial electrolysis (Redox reaction) resulting in a significant bubble formation.

For a single pulse and 20 V magnitude, pulse width of 100 ms caused severe damage to cell membrane with a large irreversible visible pore, whereas smaller pulsewidths only caused EP or no effect was observed. With larger pulsewidths (500 ms or more) with the same applied potential, cellular structures were observed to be disintegrated or completely destroyed. For instance, Fig. 7(a) shows many visible stained cell structures prior to pulse application (0 s), and Fig. 7(b) shows few cell structures immediately after the pulse application (0.5 s). The dissipation of pink stain in the buffer medium is suggestive of the Eosin Y stained cytoplasm being dispersed in the buffer fluid. With increased pulsewidth of 1 s, cell structures were observed to be completely disintegrated (see Fig. 8). The probability of the cells being completely hidden under bubbles is low, as depicted in Fig. 8(c), which is a superimpose of Fig. 8(a) on the inversion of Fig. 8(b).

TABLE I
SUMMARY OF OBSERVATIONS WITH VARIOUS ELECTRICAL EXCITATION PARAMETERS

Applied potential (V)	Pulse width (s)	Number of pulses	Total time of excitation (s)	Observation (FI of EP)
2.5	1×10^{-6}	10	10×10^{-6}	No EP or EL
2.5	1×10^{-3}	10	10×10^{-3}	No EP or EL
5	1×10^{-6}	1	1×10^{-6}	No EP or EL
5	1×10^{-6}	10	10×10^{-6}	No EP or EL
5	100×10^{-6}	1	100×10^{-6}	No EP or EL
5	10×10^{-6}	100	1×10^{-3}	No EP or EL
5	1×10^{-3}	1	1×10^{-3}	EP (0.0661)
5	1×10^{-3}	10	10×10^{-3}	EP (0.1306)
5	1×10^{-3}	25	25×10^{-3}	EP (0.1904)
5	10×10^{-3}	1	10×10^{-3}	EP (0.1497)
10	10×10^{-6}	1	10×10^{-6}	No EP or EL
10	100×10^{-6}	1	100×10^{-6}	No EP or EL
10	1×10^{-3}	10	10×10^{-3}	EP (0.1851)
10	10×10^{-3}	1	10×10^{-3}	EP (0.2225)
10	100×10^{-3}	1	100×10^{-3}	EP (0.3596)
15	1×10^{-3}	10	10×10^{-3}	EP (0.2472)
15	10×10^{-3}	1	10×10^{-3}	EP (0.3251)
15	100×10^{-3}	1	100×10^{-3}	EP (0.4805)
20	1×10^{-6}	1	1×10^{-6}	No EP or EL
20	1×10^{-6}	2	2×10^{-6}	No EP or EL
20	1×10^{-6}	10	10×10^{-6}	No EP or EL
20	10×10^{-6}	1	10×10^{-6}	EP (0.0516)
20	10×10^{-6}	10	100×10^{-6}	EP (0.1180)
20	10×10^{-6}	100	1×10^{-3}	EP (0.1821)
20	1×10^{-3}	1	1×10^{-3}	EP (0.2660)
20	1×10^{-3}	10	10×10^{-3}	EP (0.3295)
20	10×10^{-3}	1	10×10^{-3}	EP (0.4220)
20	10×10^{-3}	10	100×10^{-3}	EP (0.6095)
20	20×10^{-3}	1	20×10^{-3}	EP (0.4932)
20	100×10^{-3}	1	100×10^{-3}	EP (0.7298)
20	500×10^{-3}	1	500×10^{-3}	EL
20	1	1	1	EL
20	5	1	5	EL

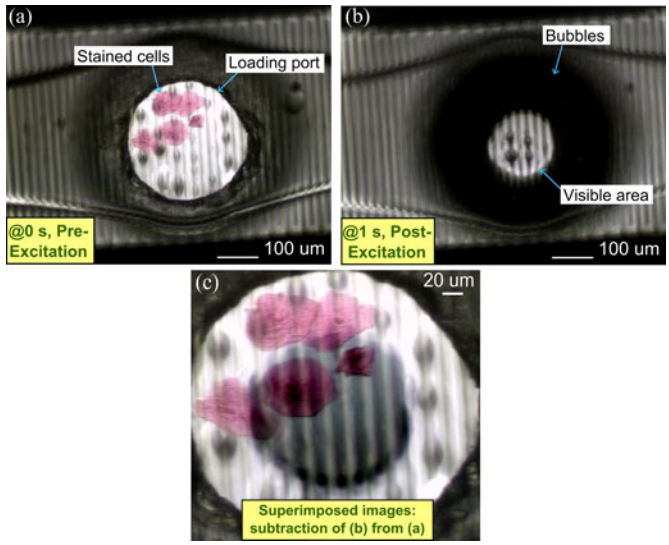

Fig. 8. Observations under a microscope after applying a single pulse of 20 V magnitude for 1 s duration. (a) Image prior to excitation (at 0 s). (b) Image immediately after excitation (at 1 s). Bubbles due to excitation limited visible area. (c) Superimposed images obtained by subtracting image (b) from image (a) and enlarged to show the loading port.

For release of DNA from inside of cells, nuclear membrane must also be ruptured in addition to plasma membrane. Nuclear membrane is a double bilayer lipid membrane. Experimental data suggest that a single pulse of 20 V amplitude for 5 s duration showed exposed DNA. Based on the internal resistance of the power supply and the voltage drop across it, the dissipated power for this condition has been calculated to be 0.4±0.1 W and the energy spent to be 2±0.5 J.

Analysis of exposed DNA is presented in Figs. 9 and 10. Fig. 9 provides two images of the same position inside the microfluidic chamber, but at two different vertical heights. The focal plane of Fig. 9(a) was at the bottom surface of the channel, whereas the focal plane of Fig. 9(b) was 10 μm vertically above. These images show the released DNA (identified with blue Haematoxylin stain) indicating that DNA was spatially distributed along the height. DNA, in the formation of chromatins, histones, and other proteins, becomes spatially distributed when nucleus membrane is broken as DNA is tightly packed in a spring-like coil formation inside the nucleus with a packing ratio of 10 000 to 1 [69].

Using ImageJ (National Institutes of Health, USA) image processing tool, the background color from Fig. 9(b) is reduced as shown in Fig. 9(e) that clearly showed the exposed DNA. This figure shows the distinctly distinguishable blue color of the Haematoxylin stains of DNA as well as the denucleated cell membranes to the right. The span of area occupied by the DNA was measured to be 45 μm, five to ten times larger than nucleus, suggesting that the DNA was uncoiled after release through EL. Observing the lysate under an optical microscope with a high magnification of 100× (oil-immersion) with optical microscope provided clear views of released DNA identified by the blue stain and the telltale sign of the extremely coiled structure of DNA (see Fig. 10).

D. Quantification Metrics

To quantify the severity of EP, a quantification metric "Flow Index of Electroporation" (FI of EP) has been defined as the amount of NSP reduction over a certain amount of time [64]. This metric can be calculated by subtracting the final value of the NSP from 1. Mathematically,

$$\text{FI of EP} = 1 - \text{Final value of the NSP.} \tag{2}$$

FI of EP is a numeric indicator of the severity of EP and relates to the amounts of fluidic exchange between an electroporated cell and its environment. A higher value of FI of EP represents higher amounts of fluidic exchange. The minimum value of FI of EP can be 0 that represents an absolute absence of EP. The maximum value of FI of EP can be 1 that might occur in the case of cell lysis. Thus, the metric provides a quantitative approach for comparison of experimental results for improved

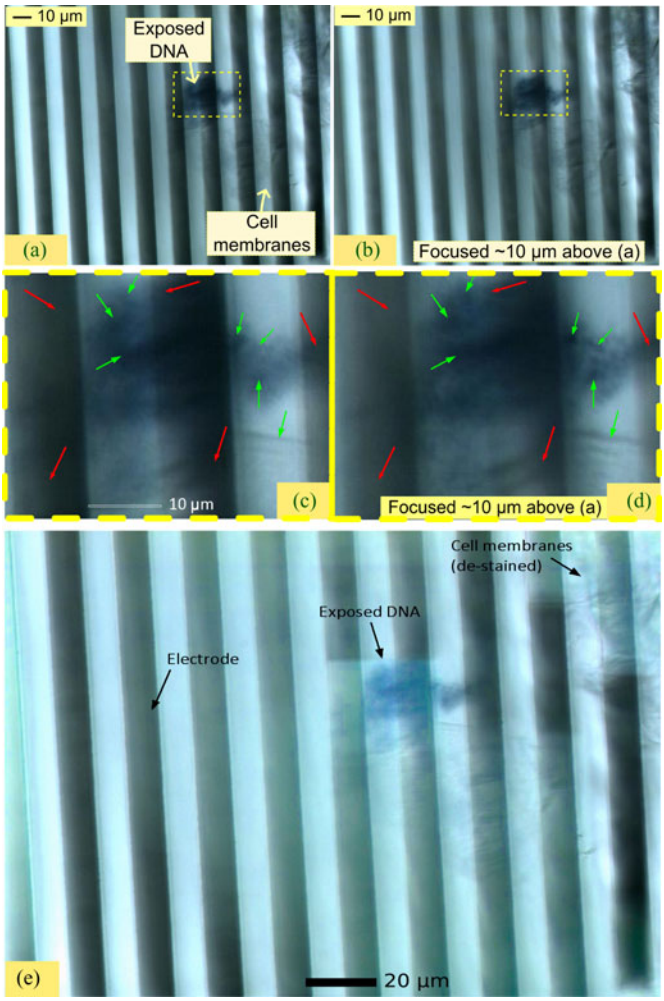

Fig. 9. (a)–(b) Two images taken from the same position, but focused at two different heights (10 μm apart), which show the released DNA through electrical lysis with an excitation of 20 V for 5 s. (c–d) Enlarged image set from the same area as in (a) and (b), respectively. The red arrows (darker and longer) indicate the spots where the contrast in the image (a) is higher than that of the image (b), whereas the green arrows (lighter and shorter) indicates vice versa. The image set demonstrates that DNA, with higher contrast in image (b), was distributed vertically inside the microchannel, whereas the electrodes with higher contrast in image (a), were located at the bottom surface of the microchannel. (e) Image of exposed DNA was filtered to reduce background using ImageJ that clearly shows stained DNA released after EL.

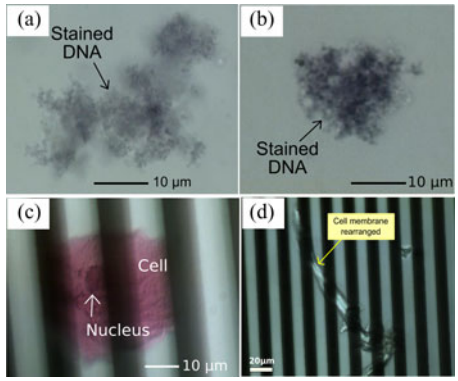

Fig. 10. (a)–(b) Two samples of the released DNA collected from the device after excitation of 20 V for 5 s, and observed under 100× objective lens with oil immersion technique in lysates collected from the device. The DNA strands are identified by the blue stain of Haematoxylin and the coiled structure that is unique to chromatins composed of DNA, histones, and other proteins. (c) Sample cell prior to lysis inside the microfluidic chamber with H&E staining is shown for a size comparison. (d) Rearranged cell membrane structures after pulse treatment with an excitation of 20 V for 5 s.

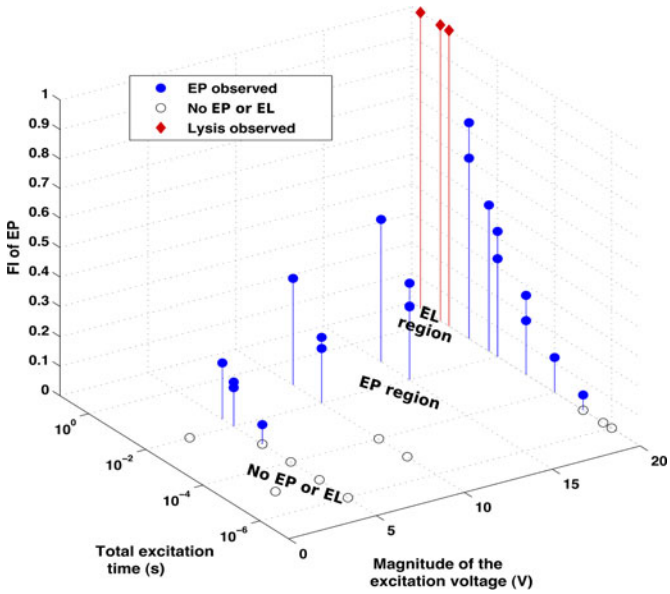

Fig. 11. Graphical representation of FI of EP versus the pulse magnitude and the total excitation time. FI of EP for no EP or EL observed, and lysis observed are denoted as 0 and 1, respectively. Note that a single pulse can be considered as the ceiling of achievable FI of EP for the energy stimulation in a given experimental condition. There are potentially three distinct regions on a total excitation time versus applied voltage surface (energy-space plot) as indicated.

classification, systematic study, quantitative analysis, and optimization of EP.

The last column values (within parenthesis) of Table I provides the list of FI of EP for various electrical pulse excitation conditions from the experiments at 145 s after the excitation. FI of EP for various excitation pulse magnitudes and total excitation time are plotted in Fig. 11. It is important to note from this figure that higher FI of EP occurs for lesser number of pulses for the same energy delivery. Thus, applying a single pulse can be considered as the ceiling of achievable FI of EP for a given energy and experimental setup. The findings elucidate to the following two exception cases of overlapping observations (see Fig. 11).

1) There are six sets of EP observations where the excitation condition (voltage and total excitation time) overlaps. We note that in each set, FI of EP is higher for lesser number of pulses, i.e., a single pulse produced higher FI of EP compared to multiple pulses delivering the same amount of energy. The differences are more prominent with higher energy pulses. As in all of the overlapping observations at the same excitation point, the single pulse case has produced the maximum FI of EP, so FI of EP due to a single pulse can be treated as the ceiling of achievable FI of EP for that amount of energy.

2) There are two sets of observations where EP observed overlap with no effect observed. The values of FI of EP for these excitation points are 0.0661 (5 V, 1 pulse of 1 ms duration) and 0.0516 (20 V, 1 pulse of 10 μs duration). Corresponding

TABLE II
SUMMARY OF EXPERIMENTAL OBSERVATIONS FOR VARIOUS APPLIED EXCITATION PARAMETERS

Applied potential	Pulse width (s)	Observation
Less than 5 V	Any	No EP or EL observed
5 V to 20 V	10 μs to 100 ms	EP (various degrees)
20 V	0.5 s to 2 s	EL
20 V	5 s or more	EL (DNA released)

excitations for "no effect observed" have multiple pulses delivering the same amount of energy (5 V, 100 pulses of 10 μs duration and 20 V, 10 pulses of 1 μs duration, respectively). In accordance to the previous scenario, a single pulse inflicted higher impact on the cell membrane resulting EP compared to "no EP or EL observed" with multiple pulses delivering the same total amount of energy.

"Degree of electroporation" term was denoted previously to refer to severity or extent of EP [70], [71]. Here, we define the degree of EP as *the ratio of the total pore area that is formed during EP to the surface area of the cell*. Using this definition, it clearly represents the extent of pore formation during the EP process and becomes an important criterion to distinguish among various cases of EP. This definition can be represented mathematically as follows:

$$\text{Degree of electroporation} = \frac{\text{Total pore area}}{\text{Cell surface area}}. \qquad (3)$$

Degree of EP represents a metric for denoting severity of EP. The significance of degree of EP is that higher degree of EP will allow higher amount of fluidic exchange through the cell membrane within a given duration in a certain buffer fluid. FI of EP has a positive correlation with degree of EP and the time duration of EP. Hence, the product of degree of EP with the corresponding EP duration can be a direct indication of the total fluidic exchange among various excitation conditions represented by FI of EP. These metrics, FI of EP, and degree of EP, allow quantitative analysis to compare EP to optimize fluidic exchange (e.g., for drug delivery).

V. DISCUSSIONS

A. Pulse Parameter Requirement for EP, EL, and DNA Release

The summary of experimental observation of EP, EL, and DNA release are given in Table II. In Fig. 11, the excitation conditions are plotted on an Euclidian surface with x-axis as the applied potential and y-axis as the total time of excitation (= pulsewidth $\times$ number of pulses). The xy-plane of this graph provides information on the energy delivered during the excitation as the bottom left corner represents the least energy delivery and the top right corner represents the highest energy delivery. This plot can be distinctly separated into three regions: 1) EL lysis region at the top right-hand corner, 2) EP region in the middle, and 3) the region where no observable effect at the bottom left-hand corner. Such observations are consistent with similar reports [16].

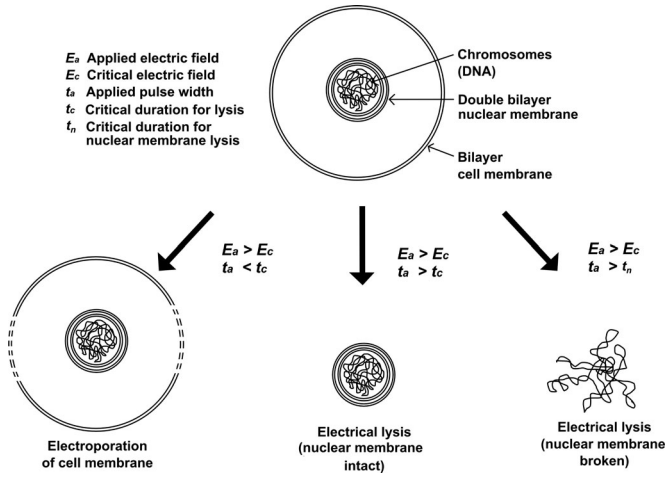

Fig. 12. Artistic sketch showing the effects of applying electric fields above the critical level with different pulsewidths on the sample cell with nucleus causing electroporation, electrical lysis, and nucleus membrane disintegration that released DNA.

Both the magnitude and the duration of the applied electric field are important criteria that determine the effect to be experienced by the cells. For micron width pulses, no visible effect of cell membrane was observed with electric field strength up to 20 kV/cm. For pulsewidths between 1 to 500 ms, EP phenomenon were detected, where narrower pulses did not cause any morphological changes in cell shape, size or orientation compared to relatively wider pulses causing significant cell membrane deformation. In all cases, for the same amount of energy delivery, single pulse caused the most significant deformation of the cell membrane. As pulses of duration over 500 ms with magnitude of 20 V were applied, cell membrane structures were destroyed causing EL. Released DNA were detected with 20 V applied potential and pulsewidths beyond 5 s. These findings are depicted with an artistic sketch in Fig. 12. From experimental data, the critical electric field E_c is 2 MV/m and the critical time for lysis t_c is 0.5 s ($N = 3$). The large duration of pulse ($t_n \approx 5$ s) required to release DNA by breaking the nuclear membrane might be due to smaller size of nucleus compared to the cell or the double bilayer lipid membrane enclosure of nucleus compared to single bilayer lipid membrane of the cell or a combination of both.

B. Comparison With Other Studies

Table III compares the features of the device in this paper with other similar devices reported in the literature. This paper is the first to use coplanar interdigitated electrode configuration for EL, which provides area coverage of up to 50%, higher than any other configurations and requires a low excitation potential. Furthermore, the position of the electrodes at the bottom of the microchannels compared to that in the sidewalls of microchannels enables the accommodation of larger (or smaller) cells with respect to the electrode spacing.

The cell samples used in this paper are human buccal cells, which are relatively large compared to virus or bacteria cells. This paper also uses a single pulse for cell lysis compared to

TABLE III
COMPARISON OF THE MICROFLUIDIC DEVICE OF THIS PAPER WITH THE LITERATURE

Feature	Lee [19]	Lu [22]	Lu [25]	Park [62]	Rosa [61]	This work
Electrode configuration	Triangular	Saw-tooth	Cylindrical	Pointed	Cylindrical	Interdigitated
Minimum electrode gap	5 μm	30 μm	20 μm	100 nm to 1.5 μm	15 μm	10 μm
Width of electrodes	14 μm	90 μm	50 μm	Unknown	50 μm	10 μm
Position of electrodes	Sidewall	Sidewall	Vertically in middle	Unknown	Sidewall	Bottom
Cell samples	Protoplasts, *E. coli*	Human colon carcinoma	Leukocytes	Vaccinia virus	*B. pertussis* bacteria	Human buccal cells
Applied potential	5 to 20 V, pulsed	8.5 V 10 kHz AC	10 V pulsed	20 V 10 kHz AC	300 V, pulsed	20 V, pulsed
Duration of excitation	100 μs to 1 ms, 5 pulses	Continuous	100 μs, 4 Hz, continuous	Unknown	9 or 324 pulses	Single pulse >0.5 s for lysis, >5 s for DNA release

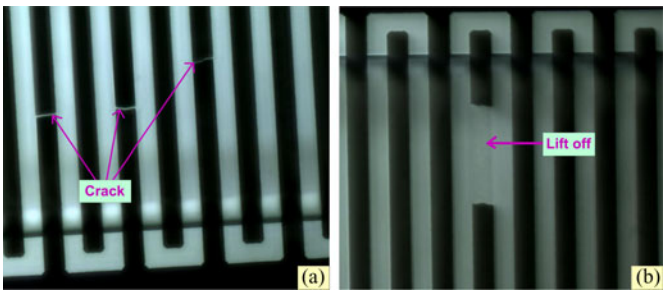

Fig. 13. Two types of defects observed in the integrated electrodes (fingers) inside the cell microfluidic chamber of the device after repeated electrical lysis experimentation: (a) Crack and (b) Lift off.

multiple pulses in other works, as our other study with EP has determined that a single pulse causes more severe damage to cell membrane compared to multiple pulses with the same energy content [64], [68]. Other techniques including electrochemical cell lysis using interdigitated integrated electrodes have been reported with lower magnitude of applied potential (e.g., 5 V) and longer time duration (e.g., 5 min) [72], in comparison to the results from our work using EL without any chemical lysis agent.

C. Reusability and Degradation

After prolonged excitation or repeated experiments, the electrodes degraded and defects were noted. Two types of defects were observed in the fingers of the interdigitated integrated electrodes (see Fig. 13).

1) *Crack:* Development of thin cracks disconnected a portion of the finger from the excitation source.

2) *Lift-off:* Portions of electrodes were completely lifted off, moved elsewhere in the channel disconnecting portions of fingers, and sometimes short-circuited adjacent fingers.

As the electrodes connected to anode side were only degraded, the electrochemical reaction might be the possible cause of such defects. If heat was the cause of such defects, both electrodes would be equally affected. Analyzing electrochemical reactions that would occur at the anode and the cathode of the interdigitated electrodes, the Tantalum (Ta) adhesion layer of the Anode terminal would turn to Tantalum Oxide (Ta_2O_5), which does not possess the adhesion properties and would dissolve causing Platinum (Pt) layer of the finger to break and to develop the above-mentioned defects.

Electrolysis of water:

Cathode: $2H_2O + 2e^- \rightarrow H_2 + 2OH^-$

Anode: $4OH^- \rightarrow O_2 + 2H_2O + 4e^-$

Dissolving of Tantalum:

Anode: $Ta + 10OH^- \rightarrow Ta_2O_5 + 5H_2O.$

D. Potential for On-Chip Integration

For LOC integration, the microfluidic chamber needs to be incorporated with other on-chip biochemical processing techniques. Various drugs can be loaded into the cell through on-chip EP. On-chip EL for DNA analysis is quite demanding, where DNA purification can be done with microbeads, and on-chip polymerize chain reaction amplification can use microreactors [73], [74] or continuous flow microchannel [75]. For sequencing of DNA on-chip, capillary electrophoresis [76], DNA microarray [77] or other solid state DNA sequencing [78] techniques can be implemented in the downstream.

VI. CONCLUSION

The developed microfluidic device has been successfully used to demonstrate EP for a range of excitation conditions with various applied voltages, pulsewidths, and number of pulses, and EL for high energy pulses, as well as DNA release with a low operating voltage of 20 V. Electric field simulations showed that electric field strength of over 20 kV/cm is developed with the application of 20 V. Thermal simulations showed that the upper bound of temperature rise of the microchannel was 1.3 °C, at 20 V excitation for 5 s, which would not influence any significant change of cell morphology. Quantitative image analysis and the quantification metric, FI of EP, allowed quantitative comparison and analysis of various excitation conditions. Higher energy delivered by higher applied voltages, longer pulse durations, and increased numbers of pulses resulted in higher FI of EP, and is consistent with other studies [46]. For the same total energy delivery, a single pulse produced higher FI of EP compared to multiple pulses. EL was observed for pulses over 0.5 s with 20 V applied potential. For release of DNA, an excitation pulse of 20 V and 5 s or longer durations were required. The method allowed quantitative analysis of EP for various electrical excitations, and thus would enable improved classification, systematic

study, quantitative analysis, and optimization of EP. On-chip EL and DNA release integrated with other microfluidic processing steps would allow development of a complete genetic analysis solution through LOC technology.

ACKNOWLEDGMENT

The authors would like to thank the anonymous reviewers and editors for their valuable comments, suggestions and insights to improve the quality of this manuscript.

REFERENCES

[1] J. M. Graham and J. A. Higgins, *Membrane Analysis*, NY, USA: BIOS Scientific, 1997.

[2] C. Yao, D. Mo, C. Li, C. Sun, and Y. Mi, "Study of transmembrane potentials of inner and outer membranes induced by pulsed-electric-field model and simulation," *IEEE Trans. Plasma Sci.*, vol. 35, no. 5, pp. 1541–1549, Oct. 2007.

[3] Q. Hu, V. Shidhara, R. P. Joshi, J. F. Kolb, and K. H. Schoenbach, "Molecular dynamics analysis of high electric pulse effects on bilayer membranes containing DPPC and DPPS," *IEEE Trans. Plasma Sci.*, vol. 34, no. 4, pp. 1405–1411, Aug. 2006.

[4] R. P. Joshi and K. H. Schoenbach, "Electroporation dynamics in biological cells subjected to ultrafast electrical pulses: A numerical simulation study," *Phys. Rev. E*, vol. 62, no. 1, pp. 1025–1033, 2000.

[5] M. Tarek, "Membrane electroporation: A molecular dynamics simulation," *Biophys. J.*, vol. 88, pp. 4045–4053, 2005.

[6] D. Moldovan, D. Pinisetty, and R. V. Devireddy, "Molecular dynamics simulation of pore growth in lipid bilayer membranes in the presence of edge-active agents," *Appl. Phys. Lett.*, vol. 91, no. 20, pp. 204 104–3, 2007.

[7] E. Neumann, A. E. Sowers, and C. A. Jordan, *Electroporation and Electrofusion in Cell Biology*. New York, NY, USA: Plenum Press, 1989.

[8] M. Fox, D. Esveld, A. Valero *et al.*, "Electroporation of cells in microfluidic devices: A review," *Anal. Bioanal. Chem.*, vol. 385, pp. 474–485, 2006.

[9] H. Fujimoto, K. Kato, and H. Iwata, "Electroporation microarrray for parallel transfer of small interfering RNA into mammalian cells," *Anal. Bioanal. Chem.*, vol. 392, pp. 1309–1316, 2008.

[10] S. Koda, Y. Inoue, and H. Iwata, "Gene transfection into adherent cells using electroporation on a dendrimer-modified gold electrode," *Langmuir*, vol. 24, no. 23, pp. 13 525–13 531, 2008.

[11] C. Ionescu-Zanetti, A. Blatz, and M. Khine, "Electrophoresis-assisted single-cell electroporation for efficient intracellular delivery," *Biomed. Microdevices*, vol. 10, pp. 113–116, 2008.

[12] H. Wang and C. Lu, "Microfluidic electroporation for delivery of small molecules and genes into cells using a common dc power supply," *Biotechnol. Bioeng.*, vol. 100, no. 3, pp. 580–586, 2008.

[13] Z. Fei, S. Wang, Y. Xie, B. Henslee, C. Koh, and L. Lee, "Gene transfection of mammalian cells using membrane sandwich electroporation," *Anal. Chem.*, vol. 79, no. 15, pp. 5719–5722, 2007.

[14] Y. Huang and B. Rubinsky, "Microfabricated electroporation chip for single cell membrane permeabilization," *Sens. Actuators*, vol. 89, pp. 242–249, 2001.

[15] J. C. Weaver, "Electroporation of cells and tissues," *IEEE Trans. Plasma Sci.*, vol. 28, no. 1, pp. 24–33, Feb. 2000.

[16] S. B. Dev, D. P. Rabussay, G. Widera, and G. A. Hofmann, "Medical applications of electroporation," *IEEE Trans. Plasma Sci.*, vol. 28, no. 1, pp. 206–223, Feb. 2000.

[17] B. I. Morshed, M. Shams, and T. Mussivand, "Electrical lysis: Dynamics revisited and advances in on-chip operation," *Crit. Rev. Biomed. Eng.*, vol. 41, no. 1, pp. 37–50, 2013.

[18] R. B. Brown and J. Audet, "Current techniques for single-cell lysis," *J. Roy. Soc. Interf.*, vol. 5, pp. S131–S138, 2008.

[19] S. W. Lee and Y. C. Tai, "A micro cell lysis device," *Sens. Actuators*, vol. 73, pp. 74–79, 1999.

[20] C. E. Sims, G. P. Li, M. R. Chang, N. Allbritton, and M. Bachman, "Fast electrical lysis of cells for capillary electrophoresis," *Analyt. Chem.*, vol. 75, no. 15, pp. 3688–3696, 2003.

[21] J. Gao, X. Yin, and Z. Fang, "Integration of single cell injection, cell lysis, separation and detection of intercellular constituents on a microfluidic chip," *Lab Chip*, vol. 4, pp. 47–52, 2004.

[22] H. Lu, M. A. Schmidt, and K. F. Jensen, "A microfluidic electroporation device for cell lysis," *Roy. Soc. Chem.*, vol. 5, pp. 23–29, 2005.

[23] H. Wang, A. K. Bhunia, and C. Lu, "A microfluidic flow-through device for high throughput electrical lysis of bacterial cells based on continuous DC voltage," *Biosens. Bioelectron.*, vol. 22, pp. 582–588, 2006.

[24] D. W. Lee and Y. Cho, "A continuous electrical cell lysis device using a low DC voltage for a cell transport and rupture," *Sens. Actuators*, vol. B 124, pp. 84–89, 2007.

[25] K. Lu, A. M. Wo, Y. Lo, K. Chen, C. Lin, and C. Yang, "Three dimensional electrode array for cell lysis via electroporation," *Elsevier Biosens. Bioelectron.*, vol. 28, no. 1, pp. 24–33, 2006.

[26] H. Kido, M. Micic, D. Smith, J. Zoval, J. Norton, and M. Madou, "A novel, compact disk-like centrifugal microfluidics system for cell lysis and sample homogenization," *Colloids Surf. B: Biointerf.*, vol. 58, pp. 44–51, 2007.

[27] P. J. Marc, C. E. Sims, M. Bachman, G. P. Lia, and N. L. Allbritton, "A microfluidic device for physical trapping and electrical lysis of bacterial cells," *Appl. Phys. Lett.*, vol. 92, pp. 214 103–3, 2008.

[28] Y. Lin and G. Lee, "An integrated cell counting and continuous cell lysis device using an optically induced electric field," *Sens. Actuators B*, vol. 145, pp. 854–860, 2010.

[29] D. Voet and J. G. Voet, *Biochemistry*, 3rd ed. New York, NY, USA: Wiley, 2004.

[30] H. Lodis, A. Berk, C. A. Kaiser, M. Krieger, A. Bretscher, H. Ploegh, A. Amon, and M. P. Scott, *Molecular Cell Biology*. New York, NY, USA: Freeman, 2003.

[31] M. Wurm and A.-P. Zeng, "Mechanical disruption of mammalian cells in a microfluidic system and its numerical analysis based on computational fluid dynamics," *Lab Chip*, vol. 12, pp. 1071–1077, 2012.

[32] D. C. Augenstein, A. J. Sinskey, and D. I. C. Wang, "Effect of shear on the death of two strains of mammalian tissue cells," *Biotechnol. Bioeng.*, vol. 13, no. 3, pp. 409–418, 1971.

[33] B. Arrojo, M. Figueroa, A. M. Corral, J. L. Campos, and R. Mendex, "Influence of gas flow-induced shear stress on the operation of the anammox process in a SBR," *Chemosphere*, vol. 72, no. 11, pp. 1687–1693, 2008.

[34] S. Razin, "Osmotic lysis of mycoplasma," *Microbiology*, vol. 33, no. 3, pp. 471–475, 1963.

[35] D. W. Lee and Y. Cho, "A continuous cell lysis device using focused high electric field and self-generated electroosmotic flow," in *Proc. IEEE Int. Conf. Micro Electro Mech. Syst.*, 2006, pp. 426–429.

[36] P. Rajasekhar, L. Fan, T. Nguyen, and F. A. Roddick, "A review of the use of sonication to control cyanobacterial blooms," *Water Res.*, vol. 46, no. 14, pp. 4319–4329, 2012.

[37] S. C. Dixon, J. Horti, Y. Guo, E. Reed, and W. D. Figg, "Methods for extracting and amplifying genomic DNA isolated from frozen serum," *Nature Biotechnol.*, vol. 16, pp. 91–94, 1998.

[38] R. Halim, R. Harun, M. K. Danquah, and P. A. Webley, "Microalgal cell disruption for biofuel development," *Appl. Energy*, vol. 91, no. 1, pp. 116–121, 2012.

[39] J. Kim, M. Johnson, P. Hill, and B. K. Gale, "Microfluidic sample preparation: Cell lysis and nucleic acid purification," *Integr. Biol.*, vol. 1, pp. 574–586, 2009.

[40] M. D. Dhawan, F. Wise, and A. J. Baeumner, "Development of a laser-induced cell lysis system," *Analyt. Bioanalyt. Chem.*, vol. 374, pp. 421–426, 2002.

[41] H. Lai, P. A. Quinto-Su, C. E. Sims, M. Bachman, G. P. Li, V. Venugopalan, and N. L. Allbritton, "Characterization and use of laser-based lysis for cell analysis on-chip," *J. Roy. Soc. Interf.*, vol. 5, pp. S113–S121, 2008.

[42] K. Zhua, H. Jin, Y. Maa, Z. Ren, C. Xiao, Z. He, F. Zhang, Q. Zhu, and B. Wang, "A continuous thermal lysis procedure for the large-scale preparation of plasmid DNA," *J. Biotechnol.*, vol. 118, pp. 257–264, 2005.

[43] S.-K. Baek, J. Min, and J.-H. Park, "Wireless induction heating in a microfluidic device for cell lysis," *Lab Chip*, vol. 10, pp. 909–917, 2010.

[44] R. W. Doebler, B. Erwin, A. Hickerson, B. Irvine, D. Woyski, A. Nadim, and J. D. Sterling, "Continuous-flow, rapid lysis devices for biodefense nucleic acid diagnostic systems," *J. Assoc. Lab. Autom.*, vol. 14, no. 3, pp. 119–125, 2009.

[45] K. Maswiwat, D. Wachner, and J. Gimsa, "Effects of cell orientation and electric field frequency on the transmembrane potential induced in ellipsoidal cells," *Bioelectrochemistry*, vol. 74, pp. 130–141, 2008.

[46] B. L. Ibey, D. G. Mixon, J. A. Payne, A. Bowman, K. Sickendick, G. J. Wilmink, W. P. Roach, and A. G. Pakhomov, "Plasma membrane perme-

abilization by trains of ultrashort electric pulses," *Bioelectrochemistry*, vol. 79, no. 114, pp. 114–121, 2010.
[47] H. Wang and C. Lu, "High-throughput and real-time study of single cell electroporation using microfluidics: Effects of medium osmolarity," *Biotechnol. Bioeng.*, vol. 95, pp. 1116–1125, 2006.
[48] R. Ziv, Y. Steinhardt, G. Pelled, D. Gazit, and B. Rubinsky, "Micro-electroporation of mesenchymal stem cells with alternating electrical current pulses," *Biomed. Microdev.*, vol. 11, pp. 95–101, 2009.
[49] A. Agarwal, I. Zudans, E. A. Weber, J. Olofsson, O. Orwar, and S. G. Weber, "Effect of cell size and shape on single-cell electroporation," *Anal. Chem.*, vol. 79, no. 10, pp. 3589–3596, 2007.
[50] C. Chen, J. A. Evans, M. P. Robinson, S. W. Smye, and P. O'Toole, "Measurement of the efficiency of cell membrane electroporation using pulsed ac fields," *Phys. Med. Biol.*, vol. 53, pp. 4747–4757, 2008.
[51] H. He, D. C. Chang, and Y. Lee, "Using a micro electroporation chip to determine the optimal physical parameters in the uptake of biomolecules in hela cells," *Bioelectrochemistry*, vol. 70, pp. 363–368, 2007.
[52] H. Wang and C. Lu, "Electroporation of mammalian cells in a microfluidic channel with geometric variation," *Anal. Chem.*, vol. 78, no. 14, pp. 5158–5164, 2006.
[53] S. M. Kennedy, Z. Ji, J. C. Hedstrom, J. H. Booske, and S. C. Hagness, "Quantification of electroporative uptake kinetics and electric field heterogeneity effects in cells," *Biophysical J.*, vol. 94, pp. 5018–5027, 2008.
[54] M. Olbrich, E. Rebollar, J. Heitza, I. Frischauf, and C. Romanin, "Electroporation chip for adherent cells on photochemically modified polymer surfaces," *Appl. Phys. Lett.*, vol. 92, pp. 013 901-1–013901-3, 2008.
[55] K. Huang, Y. Lin, K. Su, and H. Chen, "An electroporation microchip system for the transfection of zebrafish embryos using quantum dots and GFP genes for evaluation," *Biomed. Microdev.*, vol. 9, pp. 761–768, 2007.
[56] J. A. Kima, K. Choa, Y. S. Shin, N. Jung, C. Chunga, and J. K. Changa, "A multi-channel electroporation microchip for gene transfection in mammalian cells," *Biosens. Bioelectron.*, vol. 22, pp. 3273–3277, 2007.
[57] N. Ikeda, N. Tanaka, Y. Yangida, and T. Hatsuzawa, "On-chip single-cell lysis for extracting intracellular material," *Japan. J. Appl. Phys.*, vol. 46, no. 9B, pp. 6410–6414, 2007.
[58] Y. Nashimoto, Y. Takahashi, and T. Yamakawa, "Measurement of gene expression from single adherent cells and spheroids collected using fast electrical lysis," *Anal. Chem.*, vol. 79, no. 7, pp. 6823–6830, 2007.
[59] N. R. Munce, J. Li, P. R. Herman, and L. Lilge, "Microfabricated system for parallel single-cell capillary electrophoresis," *Analyt. Chem.*, vol. 76, no. 17, pp. 4983–4989, 2004.
[60] P. J. Marc, C. E. Sims, M. Bachman, G. P. Lia, and N. L. Allbritton, "Fast-lysis cell traps for chemical cytometry," *Lab Chip*, vol. 8, pp. 710–716, 2008.
[61] C. Rosa, P. A. Tilley, J. D. Fox, and K. V. Kaler, "Microfluidic device for dielectrophoresis manipulation and electrodisruption of respiratory pathogen *bordetella pertussis*," *IEEE Trans. Biomed. Eng.*, vol. 55, no. 10, pp. 2426–2432, Oct. 2008.
[62] K. Park, D. Akin, and R. Bashir, "Electrical capture and lysis of vaccinia virus particles using silicon nano-scale probe array," *Biomed. Microdev.*, vol. 9, pp. 877–883, 2007.
[63] S. J. Beebe, P. M. Fox, L. J. Rec, K. Somers, R. H. Stark, and K. H. Schoenbach, "Nanosecond pulsed electric field (nsPEF) effects on cells and tissues: Apoptosis induction and tumor growth inhibition," *IEEE Trans. Plasma Sci.*, vol. 30, no. 1, pp. 286–292, Feb. 2002.
[64] B. I. Morshed, M. Shams, and T. Mussivand, "Identifying severity of electroporation through quantitative image analysis," *Appl. Phys. Lett.*, vol. 98, pp. 143704-1–143704-3, 2011.
[65] U. Danielsson, "Convective heat transfer measured directly with a heat flux sensor," *Amer. Physiol. Soc.*, vol. 68, no. 3, pp. 1275–1281, 1990.
[66] J. P. Holman, *Heat Transfer*. Columbus, OH: McGraw-Hill, 2009.
[67] J. H. Hienhard IV, J. H. Hienhard V, *A Heat Transfer Textbook*, Cambridge, MA: Phlogiston Press, 2008.
[68] B. I. Morshed, M. Shams, and T. Mussivand, "Effectiveness of multiple pulses on flow index of electroporation," in *Proc SPIE*, 2012, vol. 8344, pp. 834 417/1–8.
[69] A. T. Annunziato, "DNA packaging: Nucleosomes and chromatin," *Nature Educ.*, vol. 1, no. 1, p. 26, 2008.
[70] J. Olofsson, M. Levin, A. Stromberg, S. G. Weber, F. Ryttsen, and O. Orwar, "Generation of focused electric field patterns at dielectric surfaces," *Anal. Chem.*, vol. 77, pp. 4667–4672, 2005.
[71] J. Olofsson, M. Levin, A. Stromberg, S. G. Weber, F. Ryttsen, and O. Orwar, "Scanning electroporation of selected areas of adherent cell cultures," *Anal. Chem.*, vol. 79, pp. 4410–4418, 2007.
[72] S. K. Jha, G.-S. Ra, G.-S. Joo, and Y.-S. Kim, "Electrochemical cell lysis on a miniaturized flow-through device," *Curr. Appl. Phys.*, vol. 9, pp. e301–e303, 2009.
[73] E. T. Lagally and R. A. Mathies, "Monolithic integrated PCR reactor-CE system for DNA amplification and analysis to the single molecule limit," in *Proc. IEEE-EMBS Microtechnol. Med. Biol.*, 2002, pp. 437–441.
[74] V. P. Iordanov, J. Bastemeijer, A. Bossche, and P.M. Sarro, "PCR array on chip for thermal characterization," in *Proc. IEEE Sens.*, 2003, vol. 2, pp. 1045–1048.
[75] M. U. Kopp, A. J. de Mello, and A. Manz, "Chemical amplification: Continuous-flow PCR on a chip," *Sci. Mag.*, vol. 280, pp. 1046–1048, 1998.
[76] B. M. Paegel, C. A. Emrich, G. J. Wedemayer *et al.*, "High throughput DNA sequencing with a microfabricated 96-lane capillary array electrophoresis bioprocessor," in *Proc. Nat. Acad. Sci.*, USA, 2002, vol. 99, pp. 574–579.
[77] M. Schienle *et al.*, "A fully electronic DNA sensor with 128 positions and in-pixel A/D conversion," *IEEE J. Solid-State Circuits*, vol. 39, no. 12, pp. 2438–2445, Dec. 2004.
[78] S. Purushothaman *et al.*, "Towards fast solid state DNA sequencing," in *Proc. IEEE Int. Symp. Circuits Syst.*, 2002, vol. IV, pp. 169–172.

Bashir I. Morshed (M'12) received the B.Sc. degree in electrical and electronics engineering from Bangladesh University of Engineering and Technology, Dhaka, Bangladesh, in 2001, the MA.Sc. degree in electrical and computer engineering from the University of Windsor, ON, Canada, in 2004, and Ph.D. degree in electrical and computer engineering from Electronics Department, Carleton University, ON, Canada, in 2010.

He was awarded the prestigious Canadian Commonwealth Fellowship. Since 2011, he has been an Assistant Professor of the Electrical and Computer Engineering, University of Memphis, TN, USA.

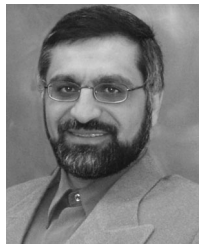

Maitham Shams is an Associate Professor in the Department of Electronics, Carleton University, ON, Canada. He received the M.A.Sc. and Ph.D. degrees in electrical and computer engineering from the University of Waterloo, Waterloo, ON, Canada, in 1994 and 1999, respectively.

His research interests include digital circuits optimization, subthreshold circuits, FinFETs, asynchronous circuits design, and medical devices.

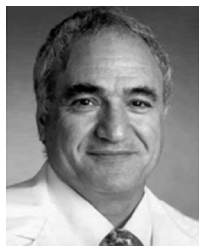

Tofy Mussivand received the undergraduate degree in engineering and management in 1963. He received the Ph.D. degree in medical engineering and medical sciences from the University of Akron and Northeastern Ohio Universities Colleges of Medicine, Rootstown, OH, USA, in 1988.

He worked in senior positions in government, crown corporations, and the private sector. He worked at the Cleveland Clinic prior to be invited to return to Canada to continue his pioneering work in various medical devices areas in 1989.